Chinese Chemical Letters 35 (2024) 108940

Contents lists available at ScienceDirect

Chinese Chemical Letters

journal homepage: www.elsevier.com/locate/cclet

Rational design of hydroxytricyanopyrrole-based probes with high affinity and rapid visualization for amyloid-β aggregates *in vitro* and *in vivo*

Jiajia Lv[a,b], Jie Gao[b,c], Hongyu Li[b,c], Zeli Yuan[b,c,*], Nan Dong[a,*]

[a] School of Chemistry and Chemical Engineering, Guizhou University, Guiyang 550025, China
[b] School of Pharmacy, Zunyi Medical University, Zunyi 563003, China
[c] Guizhou International Scientific and Technological Cooperation Base for Medical Photo-Theranostics Technology and Innovative Drug Development, Zunyi 563003, China

ARTICLE INFO

Article history:
Received 2 June 2023
Revised 10 August 2023
Accepted 16 August 2023
Available online 19 August 2023

Keywords:
Amyloid-β
Fluorescent probe
Hydroxytricyanopyrrole
Fluorescence imaging
Alzheimer's disease

ABSTRACT

As key biomarkers, amyloid-β (Aβ) plaques are frequently used to diagnose Alzheimer's disease (AD). Although fluorescence imaging has proven to be effective in detecting these plaques, the gold standard probe thioflavin T (ThT), used for Aβ aggregates, cannot be applied *in vivo* owing to its invasive nature. Therefore, the development of novel fluorescent probes capable of identifying Aβ plaques *in situ* is necessary. Based on the ThT structure, two π-conjugated heterocyclic D-π-A probes were designed bearing the hydroxytricyanopyrrole acceptor and *N*,*N*-dimethylaminophenyl donor. These probes exhibited red to near-infrared fluorescence emission (λ_{max} = 732 nm), large Stokes shifts (>100 nm), exceptional signal-to-noise ratio, rapid response (<30 s), and high binding affinity (NT-HTCP = 33.32 nmol/L; NF-HTCP = 53.35 nmol/L) for Aβ aggregates. As the best candidate, NT-HTCP was used for *in situ* imaging of Aβ plaques in AD mouse models. Furthermore, *in vivo* research demonstrated that NT-HTCP could cross the blood–brain barrier and continue imaging the Aβ plaques with a good signal-to-noise ratio. Additionally, the outcomes of the docking computations helped guide the development of the Aβ probes. This study expands the family of *N*,*N*-dimethylaminophenyl-based Aβ-sensitive fluorophores, with NT-HTCP emerging as a highly promising imaging agent.

Alzheimer's disease (AD) is a devastating neurodegenerative disease that slowly erodes human health and quality of life [1]. The amyloid cascade hypothesis suggests that the deposition and accumulation of amyloid-β (Aβ) plaques in the brain, similar to photogenic fibril formation, serve as crucial pathological markers for early-stage AD diagnosis [2–6]. Diagnosing and initiating AD treatment upon detection of deposited Aβ, despite the considerable time lag between detection and the onset of cognitive dysfunction, presents an optimistic prospect [7]. However, accurately and reliably visualizing Aβ plaques poses a critical challenge that must be overcome. Postmortem detection of Aβ plaques in brain tissue indicates AD progression. For histological and pathological research on AD, accurate and sensitive detection of this insoluble analyte is essential to enhance the quantification and identification of neuropathological injury [8].

Traditional imaging methods for Aβ plaques, such as single-photon emission computed tomography [9], positron emission tomography [10], and magnetic resonance imaging [11], face difficulties in achieving a non-invasive, high-resolution, highly sensitive, and timely diagnosis of early-stage AD. Among the current tools for visualizing Aβ plaques, fluorescence imaging, a non-invasive imaging technique, is a cost-effective and convenient means of detection (Table S1 in Supporting information) [12–28]. In general, an ideal fluorescent probe for detecting Aβ plaques *in vivo* should possess the following properties: high affinity and selectivity for Aβ aggregates, excellent ability to penetrate the blood–brain barrier (BBB), near-infrared (NIR) fluorescence emission with a large Stokes shift, and good biocompatibility [11–14]. Commercially available fluorescent probes for staining Aβ plaques in clinical *in vitro* settings include thioflavin T (ThT) and thioflavin S (ThS) derivatives. However, their application for *in vivo* Aβ plaque imaging is significantly hindered by inherent limitations, such as a short emission wavelength (~480 nm) and poor BBB permeability. AOI987 was the first probe used for *in vivo* Aβ plaque imaging;

* Corresponding authors.
E-mail addresses: zlyuan@zmu.edu.cn (Z. Yuan), ndong@gzu.edu.cn (N. Dong).

https://doi.org/10.1016/j.cclet.2023.108940
1001-8417/

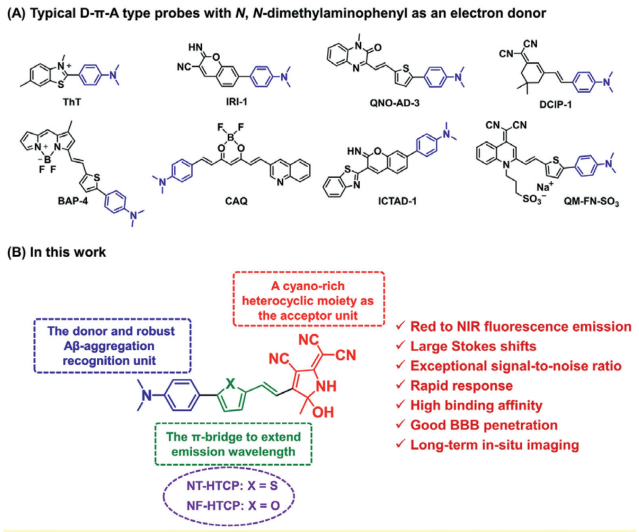

Fig. 1. (A) Typical D-π-A probes with *N*,*N*-dimethylaminophenyl as an electron donor for detecting Aβ protein aggregates. (B) Schematic diagram of novel NX-HTCP probes for Aβ protein aggregates.

however, its ionic nature prevents rapid BBB penetration [15]. Although numerous probes have been reported for Aβ plaque detection, *in situ* imaging of Aβ plaques remains challenging [12–21,29–43]. Therefore, developing and preparing high-quality i*n situ* probes for visualizing Aβ *in vivo* remain necessary.

Despite the many limitations associated with the *in vivo* use of ThT or ThS, their unique structural features hold significant value in developing novel probes because of their relatively exceptional affinity and selectivity for Aβ plaques (Table S1) [12–26]. Among these features, the *N*,*N*-dimethylaminophenyl fragment is of utmost importance and may serve as a universally accepted recognition group, facilitating enhanced binding affinity for Aβ aggregates. Based on the structural features of ThT, different fluorescent probes containing this motif have been conceived and implemented for the *in vivo* imaging of protein aggregates [12–26]. A common strategy involves constructing D-π-A-type probes, where *N*,*N*-dimethylaminophenyl acts as an ideal electron donor with π-bridges and electron-deficient units (Fig. 1). To develop NIR fluorescent probes for Aβ aggregates, a novel class of hydroxytricyanopyrrole (HTCP)-based probes, NX-HTCPs, was developed. These probes possess a high affinity for Aβ aggregates, satisfactory BBB permeability, extended retention time, and favorable biocompatibility for *in vivo* Aβ plaque imaging. To incorporate a superior binding affinity for Aβ aggregates, *N*,*N*-dimethylaminophenyl was included as a recognition group in the structure of the designed probes. HTCP, a cyano-rich heterocyclic moiety, served as a potent electron acceptor [44]. Finally, *N*,*N*-dimethylaminophenyl bridged HTCP through π-conjugated heterocycles to form red to NIR emitting D-π-A-type probes, referred to as NX-HTCPs (Fig. 1). Notably, pentameric rings featuring distinct heteroatom substitutions can significantly impact the binding of the probe to hydrophobic grooves or ridges, as well as its lipophilicity. These factors may improve the imaging performance of the resulting probes for Aβ aggregates. Here, the results of this study are presented.

The HTCP acceptor was synthesized following a previous study [45]. The donor was linked to the π-bridge through a Pd-catalyzed Suzuki–Miyaura cross-coupling reaction between boronated pentaheterocyclic aldehydes and 4–bromo-*N*,*N*-dimethylaniline [36,46]. Subsequently, novel D-π-A fluorescent probes, NX-HTCPs, were obtained through an ammonium acetate–catalyzed Knoevenagel condensation reaction with the modified donors. N-HTCP was prepared as a control probe by condensing HTCP with 4-dimethylaminobenzaldehyde [44]. The synthetic route and purification methods for both NX-HTCPs and N-HTCP are depicted in Schemes S1 and S2 (Supporting information), respectively. Detailed characterization data, including nuclear magnetic resonance (NMR) and high resolution mass spectrometry (HRMS), are provided in the experimental section and supporting information (Figs. S1–S9 in Supporting information).

The design feasibility of the probe was initially validated through theoretical calculations performed on NX-HTCPs using density functional theory (DFT) (Fig. S10 in Supporting information). The calculations revealed that the *N*,*N*-dimethylaminophenyl group, serving as an electron donor, contained most of the electrons in the highest occupied molecular orbital (HOMO), whereas the HTCP moiety, acting as an electron acceptor, contained most of the electrons in the lowest unoccupied molecular orbital (LUMO). This electron transfer from the *N*,*N*-dimethylaminophenyl unit to the HTCP unit supported the successful construction of fluorescent probes. Furthermore, the energy gaps between HOMO and LUMO for NX-HTCPs were similar (Δ_E(NT-HTCP) = 2.04; Δ_E(NF-HTCP) = 2.08), indicating that the pentameric heterocyclic ring limitedly impacted the overall electron distribution. N-HTCP exhibited the same electron distribution as the D-A structure but had a larger energy gap value than NX-HTCP (Δ_E(N-HTCP) = 2.54), resulting in a shorter fluorescence emission wavelength.

The optical properties of NX-HTCPs and N-HTCP were evaluated, as shown in Fig. S11 and Table S2 (Supporting information). The absorbance and excitation wavelengths were determined using the available NX-HTCPs, demonstrating high molar absorption coefficients and dependence on solvent polarity (with variations of up to 15 nm). The emission wavelengths also exhibited significant changes in different solvents, with an increase in solvent polarity inducing a shift in the emission wavelength from 590 nm to 735 nm. A difference of 150 nm was observed between toluene and dimethyl sulfoxide (DMSO), confirming the presence of an intramolecular charge transfer (ICT) system. Additionally, a large Stokes shift of 100–250 nm was calculated for NX-HTCPs, which is favorable for reducing background interference in bioimaging. To assess the fluorescence performance of NX-HTCPs regarding viscosity, experiments were conducted using glycerol solutions (0–90%, v/v). The fluorescence intensity of NX-HTCPs gradually increased with increasing glycerol concentration, reaching a maximum of 90% (NT-HTCP = 43.3-fold; NF-HTCP = 19.9-fold). This finding implies that the fluorescence of NX-HTCPs was influenced by viscosity (Fig. S12 in Supporting information). Moreover, the emission spectra of NX-HTCPs exhibited varying degrees of blue shift (NT-HTCP = 819 nm→787 nm; NF-HTCP = 816 nm→783 nm), possibly because of the increasing difficulty in forming the twisted ICT state of NX-HTCPs with higher glycerol concentrations [47]. The similarity of the optical properties of NX-HTCPs indicated that the pentameric heterocycles limitedly affected the absorption and fluorescence spectra. In conclusion, the NX-HTCPs showed promise as effective fluorescent probes, possessing high molar absorption coefficients, red to NIR emission wavelengths, and low fluorescence quantum yields (in EtOH solution).

The fluorescence responses of NT-HTCP, NF-HTCP, N-HTCP, and ThT were assessed before and after binding to Aβ aggregates (Fig. 2A, Figs. S13 and S14 in Supporting information). After adding the ThT solution to the prepared Aβ aggregates, a significant increase in the fluorescence signal was observed, confirming the successful preparation of Aβ aggregates, as supported by transmission electron microscopy imaging (Fig. S15 in Supporting information). The standard curves and limits of detection (LODs) for the three probes were also established against Aβ aggregates (Fig. S14). The LODs for NT-HTCP, NF-HTCP, and N-HTCP were 16, 22, and 49 nmol/L, respectively. This initial evaluation provided crucial information on the ability of NX-HTCPs to interact with Aβ aggregates. The bind-

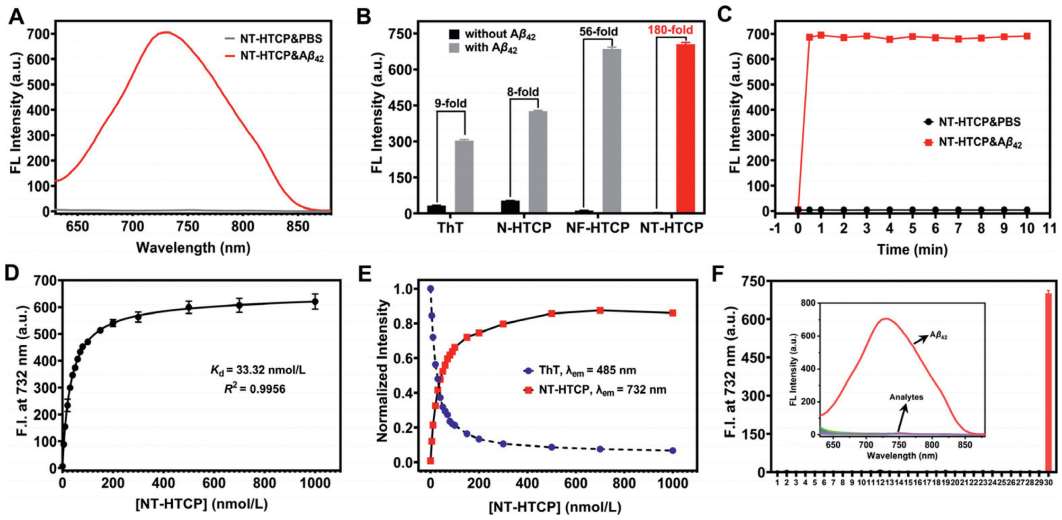

Fig. 2. (A) Fluorescence spectra of NT-HTCP (2 μmol/L) bound/unbound to Aβ_{42} aggregates (10 μmol/L). λex = 600 nm. (B) Fluorescence intensity of the probes (2 μmol/L) at the maximum wavelength (λ_{ThT} = 480 nm, $\lambda_{N\text{-}HTCP}$ = 631 nm, $\lambda_{NF\text{-}HTCP}$ = 731 nm, and $\lambda_{NT\text{-}HTCP}$ = 732 nm) in the absence and presence of Aβ aggregates (10 μmol/L). (C) The fluorescence intensity changes of NT-HTCP at 732 nm *versus* time in the absence and presence of Aβ aggregates (10 μmol/L). (D) The fluorescence titration of NT-HTCP with Aβ aggregates (10 μmol/L) using a saturation binding model. (E) NT-HTCP (0–1 μmol/L) replaced ThT in the ThT/Aβ (2 μmol/L/10 μmol/L) aggregate complex. (F) The fluorescence response of NT-HTCP to various potential interferers: 1: NT-HTCP (2 μmol/L); 2–12: metal ions (10 μmol/L; 2: Cu^{2+}, 3: Zn^{2+}, 4: Ba^{2+}, 5: Ca^{2+}, 6: K^{+}, 7: Mg^{2+}, 8: Na^{+}, 9: Ni^{2+}, 10: Fe^{3+}, 11: Al^{3+}, 12: Fe^{2+}); 13–26: amino acids (10 μmol/L; 13: Ala, 14: Arg, 15: Asp, 16: Glu, 17: His, 18: Ile, 19: Leu, 20: Lys, 21: Met, 22: Phe, 23: Pro, 24: Thr, 25: Try, 26: Val); 27–29: thiols (10 μmol/L; 27: Cys, 28: Hcy, 29: GSH); and 30: Aβ_{42} aggregates (10 μmol/L). All the experiments mentioned above were conducted in phosphate-buffered saline (pH 7.4); λ_{em} = 732 nm. Error bars: mean ± standard deviation (SD) (n = 3).

ing of NX-HTCPs to Aβ aggregates resulted in a significant increase in fluorescence emission at approximately 730 nm with a minimal wavelength shift. The fluorescence response results of NX-HTCPs in environments with different solvents or viscosities indicated that, after complexation with Aβ aggregates, NX-HTCPs were exposed to an ether (or 1,4-dioxane)-like polar environment (λ_{Em}(NT-HTCP) = ~724 nm; λ_{Em}(NF-HTCP) = ~723 nm) provided by the Aβ aggregates, which limitedly influenced their conformational freedom. This was supported by the observed fluorescence emission of NX-HTCPs at ~808 nm in a viscous environment. Notably, NT-HTCP exhibited a remarkable surge in fluorescence intensity at 732 nm, increasing by a staggering 180-fold when Aβ aggregates were introduced, with minimal initial background (Fig. 2B). Moreover, the fluorescence quantum yields of NT-HCTP before and after interaction with Aβ_{42} aggregates were determined to be 0.0434% and 5.816%, respectively. After binding with the Aβ_{42} aggregates, the fluorescence quantum yield of NT-HCTP increased by approximately 134-fold, which was favorable for subsequent *in vivo* imaging. Conversely, the fluorescence intensity of NF-HTCP only increased 56-fold in response to the same stimulus (Fig. 2B). The superiority of NT-HTCP over NF-HTCP might be attributed to differences in their responses to polar environments, with NT-HTCP being more sensitive to changes in polarity. In the investigation of the quantitative effects of polarity, the dipole moment differences for NT-HTCP and NF-HTCP were calculated to be 7.94 D and 6.91 D, respectively, using the Lippert–Mataga equation [48]. The response times of the three probes to Aβ aggregates also differed (Fig. 2C and Fig. S16 in Supporting information). NT-HTCP and NF-HTCP reached a balance in fluorescence within 0.5 min, while N-HTCP took slightly longer to stabilize at 3 min.

The dissociation constants (K_d) of NT-HTCP, NF-HTCP, and N-HTCP were determined quantitatively through fluorescence titration using a saturation binding model to be 33.32, 53.35, and 117.6 nmol/L, respectively (Fig. 2D and Fig. S17 in Supporting information). Additionally, a displacement assay for ThT-bound Aβ aggregates was performed to compare the performance of the three probes with that of commercial ThT (Fig. 2E and Fig. S18 in Supporting information). The addition of NX-HTCPs and N-HTCP to ThT-bound Aβ aggregates induced a significant decrease in ThT fluorescence intensity at 480 nm and a considerable increase in the emission peaks of the corresponding probes, effectively removing ThT with an efficiency of 80%. The competitive titration results suggested that NX-HTCPs and N-HTCP could compete for the same binding sites as ThT and that both exhibited higher binding affinities for Aβ aggregates than for ThT. Finally, the specificity of NX-HTCPs and N-HTCP for Aβ aggregates was evaluated, which showed that they were minimally affected by other potential interferers, with NT-HTCP exhibiting the best performance (Fig. 2F and Fig. S20 in Supporting information). Challenging tests were conducted to examine the fluorescence response of NT-HTCP to other typical proteins, such as lysozyme, a-synuclein, and Tau aggregates (Fig. S19 in Supporting information). NT-HTCP still exhibited good selectivity for Aβ_{42} aggregation. Clearly, NT-HTCP and NF-HTCP demonstrated excellent potential for identifying Aβ aggregates with low LOD values, high binding affinity, and high selectivity. Furthermore, the fluorescence intensity of NT-HTCP at 732 nm increased with the prolonged incubation time of Aβ monomers (Fig. S21 in Supporting information). However, owing to negligible changes in the fluorescence spectrum other than the increased fluorescence intensity, further modifications to NT-HTCP were required to better monitor the aggregate formation process. Overall, NT-HTCP showed superior recognition performance compared to NF-HTCP for Aβ aggregates, making it more suitable for *in vitro* and *in vivo* observation of Aβ plaques owing to its NIR emission and high signal-to-noise ratio.

To investigate the interaction of the three probes with Aβ aggregates, molecular docking was used. Molecular docking algorithms significantly enhanced the ability to simulate the binding between designed probe molecules and target proteins, providing a reliable understanding of the binding pattern and strength, as well as guiding the selection of the optimal molecule for subsequent experimentation. In this study, the structure of Aβ_{42} (PDB ID: 5OQV) was obtained through cryo-electron microscopy and utilized as a protein scaffold for molecular docking [49]. The docking results revealed the two most probable binding modes, and the corresponding binding affinities were determined (Figs. S22–S25 in Support-

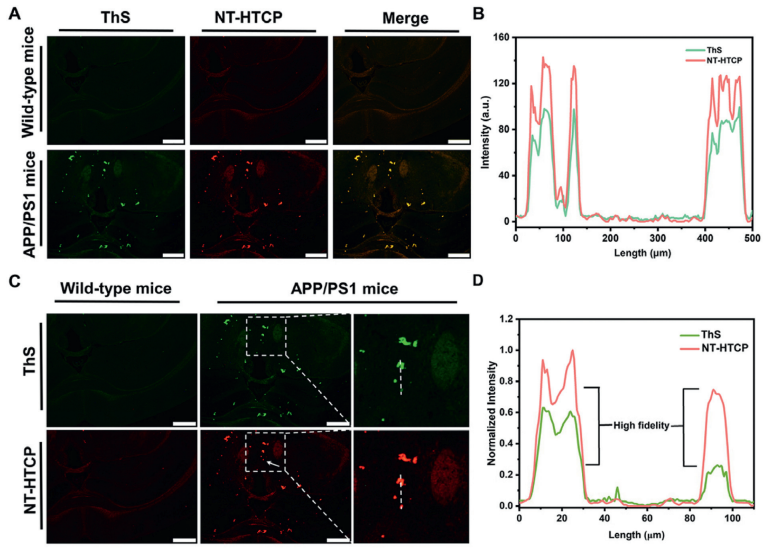

Fig. 3. (A, C) Histological staining in the hippocampus of WT and APP/PS1 transgenic mice (AD model). ThS and NT-HTCP were used as staining agents for WT and transgenic mice, respectively. (B, D) The intensity profiles of linear regions of interest that intersect the brain sections. Scale bar = 500 μm.

ing information). For NT-HTCP, Site A, situated in a tunnel along the fiber axis, was found to comprise amino acid residues, including Asn27, Ala30, Gly29, Ile31, Lys28, and Phe19, which formed a hydrophobic cavity. Site B, situated in a groove along the fiber axis surface, was in proximity to the Ala21, Glu22, and Phe20 residues. The docking score of NT-HTCP at Site A (−10.1 kcal/mol) was notably higher than the scores for the other two probe molecules (NF-HTCP = −8.6 kcal/mol; N-HTCP = −7.8 kcal/mol) and the commercial ThT (−8.8 kcal/mol). This result indicated that NT-HTCP exhibited superior binding affinity to Aβ aggregates compared to the other probes. At Site B, the docking scores for NT-HTCP, NF-HTCP, and N-HTCP were −7.9, −7.7, and −7.2 kcal/mol, respectively, indicating similar affinities to the protein. These values were lower than those of the commercially available probe ThT (Table S3 in Supporting information). It was hypothesized that the binding affinity of NX-HTCP and N-HTCP molecules was superior to that of ThT at Site B. The molecular docking results further suggested that among the three probes, NT-HTCP showed exceptional binding affinity and kinetic stability within the hydrophobic cavity of the Aβ aggregate. Additionally, they showed that NT-HTCP and the other probes had a stronger propensity to interact with Site A (a tunnel). For NT-HTCP, the docking score (binding energy) at Site A (−10.1 kcal/mol) was higher than at Site B (−7.9 kcal/mol). The minimum binding energy calculated from the docking studies indicated that NT-HTCP could interact with the residues at Site A and form the most stable complex. The negative binding free energy values suggested that the binding of NT-HTCP to Site A was spontaneous. A thorough analysis was conducted to investigate the molecular interactions between NT-HTCP and the amino acid residues at the two binding sites. Specifically, the amino acid residues surrounding the binding sites were analyzed to elucidate the mechanism of ligand binding to the protein. Unlike NF-HTCP and N-HTCP, NT-HTCP not only exhibited a distinct ability to generate van der Waals forces, carbon–hydrogen interactions, and amide-π stacking with Aβ aggregates but also established additional hydrogen bonding interactions. These results demonstrated that the modification of the heteroatom within the pentacyclic ring significantly affected the binding behavior of the probe toward Aβ aggregates. Overall, the molecular docking results were consistent with the experimental findings and provided additional insight into the complexation patterns between the probes and Aβ aggregates.

In vitro fluorescent staining was performed to evaluate the performance of NT-HTCP as an alternative to commercial probes for detecting Aβ plaques. As expected, Aβ plaques in the brain tissues of wild-type (WT) or APP/PS1 mice were specifically stained by NT-HTCP (Fig. 3A). The Animal Ethics Committee of Zunyi Medical University approved all animal studies conducted in this research project (No. Lunshen[2020]2–104) in accordance with the guidelines governing the care and use of laboratory animals. Furthermore, the presence and abundance of Aβ plaques closely matched those observed in adjacent brain sections stained with ThS (Pearson's coefficient = 0.977; overlap coefficient = 0.980), whereas no plaque labeling was observed in the brain tissues of WT mice (Fig. 3B). Notably, NT-HTCP showed richer Aβ plaque feedback than ThS. Compared to ThS, NT-HTCP could amplify the fidelity signal (arrows point to positions in Figs. 3C and D). These *in vitro* results confirmed that NT-HTCP could provide high-fidelity imaging of Aβ plaques in brain tissues.

The penetration of NT-HTCP through the BBB was initially investigated using an *in vitro* Transwell model with HCMEC/D3 and U118MG cells [50]. The fluorescence in the bottom dish was pleasing after adding NT-HTCP to the Transwells (Fig. S26 in Supporting information), indicating the potential of NT-HTCP to penetrate the BBB.

Following the simulation results of the *in vitro* BBB penetration, NT-HTCP was applied to the *in vivo* imaging of Aβ aggregates. An intravenous injection of NT-HTCP (2 mg/kg) was administered to the WT and APP/PS1 transgenic mice to monitor the fluorescence signal in their brain tissues. Fluorescence signals were detected in the brains of the mice as early as 5 min after administration, with higher intensity observed in AD mice than in WT mice (Figs. 4A and B).

Throughout the assessed experimental time points, the fluorescence signal showed a significant increase in AD mice compared to WT mice, particularly at the 30-min time point (Fig. 4C). The fluorescence intensity in the intracerebral region was recorded continuously from 5 min to 120 min post-injection, and the intensity levels observed in AD mice remained consistently and significantly higher than the peak fluorescence intensity observed in WT mice at 30 min. This result indicates the specific *in vivo* binding of NT-HTCP to Aβ plaques and its prolonged retention. *Ex vivo* imaging was also conducted to eliminate the possibility of nonspecific signal interference from other tissues. The results showed a

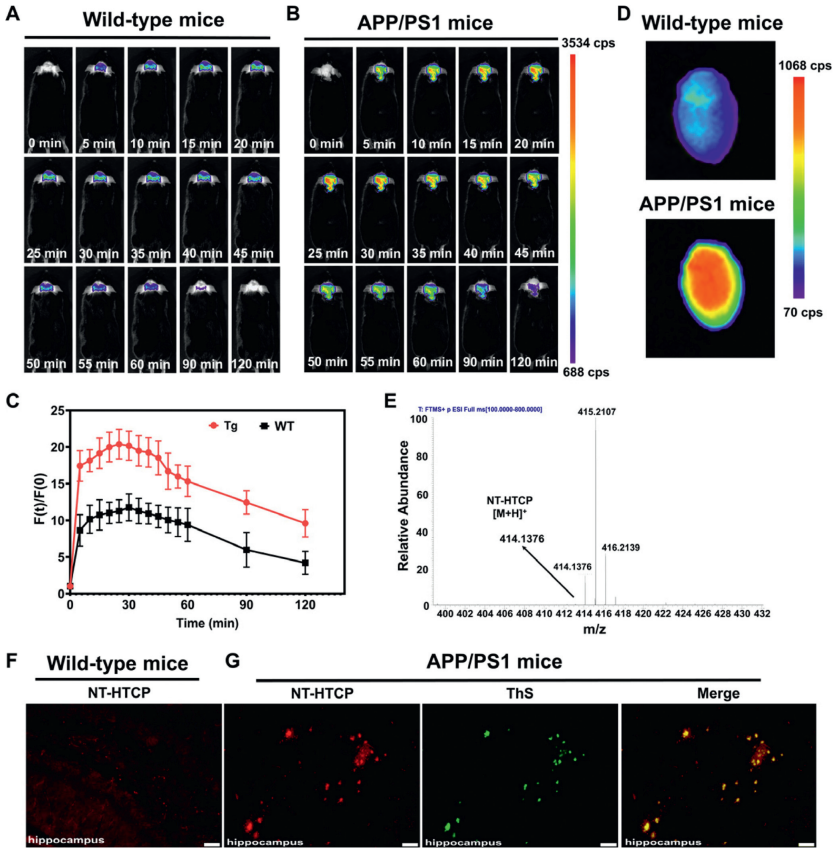

Fig. 4. *In vivo* brain images obtained from (A) WT and (B) APP/PS1 mice at various representative time points before and after the intravenous administration of NT-HTCP (2 mg/kg). (C) The relative fluorescence signal [F(t)/F(0)] in the brain regions of WT and APP/PS1 mice at different time points ($n = 3$, $P < 0.05$). Tg, APP/PS1 mice. (D) *Ex vivo* images of the brains of WT and APP/PS1 mice after the intravenous injection of 2 mg/kg NT-HTCP for 25 min. (E) A high-resolution mass spectrum obtained from brain tissue extracted from WT mice after 25 min of intravenous injection of the NT-HTCP probe. (F) *Ex vivo* fluorescent staining image of hippocampus sections obtained from WT mice after intravenous injection of NT-HTCP. (G) *Ex vivo* fluorescent staining images of the hippocampus of APP/PS1 mice after NT-HTCP intravenous injection and histological staining using ThS. Scale bar = 50 μm.

significantly higher brain signal in the AD mice compared to the WT mice (Fig. 4D). Additionally, high-resolution mass spectrometry was used to verify the penetrability of the BBB in the WT mice. The data clearly showed the presence of a peak at *m/z* 414.1376 (corresponding to $[NT\text{-}HTCP+H]^+$), confirming the BBB penetrability of NT-HTCP (Fig. 4E). Subsequently, the specific binding of NT-HTCP to Aβ plaques was further validated through *ex vivo* fluorescence staining (Figs. 4F and G). After tail vein injection, the animals were killed, and fresh frozen sections were collected from the AD and WT mice at 25 min. Fluorescence microscopy revealed numerous Aβ plaques with a high signal-to-noise ratio in hippocampus sections from AD mice (APP/PS1), and the presence of Aβ plaques in the same sections was further confirmed through ThS colocalization staining (Fig. 4G). Conversely, no significant plaques were observed in the brain sections of the WT mice (Fig. 4F).

The direct visualization results obtained in this study provide clear evidence supporting the ability of NT-HTCP to effectively label Aβ aggregates *in vivo* by crossing the BBB. Additionally, the safety of NT-HTCP was evaluated (Figs. S27–S29 in Supporting information). Results from cell MTT assays, various serum biochemical parameters, and hematoxylin-eosin (H&E) staining of the main organs demonstrated that NT-HTCP can be safely used for *in vivo* imaging of Aβ aggregates.

To achieve high-fidelity determination of Aβ plaques *in vivo*, this study aimed to develop NIR fluorescent probes that overcome the inherent limitations of commercially available probes, such as ThT and ThS. Thus, two novel probes called NX-HTCPs, which emit red to NIR fluorescence, were developed and evaluated. All NX-HTCPs exhibited enhanced fluorescence intensity at 730 nm in the emission spectrum when binding to Aβ aggregates owing to the HTCP chromophore. Among the probes, NT-HTCP displayed an exceptional signal-to-noise ratio in the fluorescence and brain tissue sections. Docking studies suggested that the N atom of cyano and the O atom of the hydroxyl group in HTCP may form supplementary hydrogen bonds with Ala31 and Lys28, respectively, leading to the enhanced performance of the probe in Aβ detection. These findings hold significant value for the Aβ probe design. Ultimately, the high imaging precision of NT-HTCP, combined with its low biotoxicity *in vivo* and its ability to localize Aβ plaques *in situ* for extended periods, provides us with ideal tools to better comprehend the pathological processes of AD and may expedite the development of promising agents for AD. Overall, this study proposes a novel approach to developing NIR fluorescence probes for the *in vivo* detection of Aβ plaques, with potential applications in advancing the understanding of AD and developing effective treatments.

Declaration of competing interest

The authors declare that they have no known competing financial interests or personal relationships that could have appeared to influence the work reported in this paper.

Acknowledgment

This work was supported by the National Natural Science Foundation of China (Nos. 22164006, 82060626, and 81360471).

Supplementary materials

Supplementary material associated with this article can be found, in the online version, at doi:10.1016/j.cclet.2023.108940.

References

[1] G. Livingston, J. Huntley, A. Sommerlad, et al., Lancet 396 (2020) 413–446.
[2] V.L. Villemagne, V. Dore, S.C. Burnham, et al., Nat. Rev. Neurol. 14 (2018) 225–236.
[3] J. Wang, C. Zhao, A. Zhao, et al., J. Am. Chem. Soc. 137 (2015) 1213–1219.
[4] P. Scheltens, B. De Strooper, M. Kivipelto, et al., Lancet 397 (2021) 1577–1590.
[5] S.J. Lee, E. Nam, H.J. Lee, et al., Chem. Soc. Rev. 46 (2017) 310–323.
[6] H. Zeng, Y. Qi, Z. Zhang, et al., Chin. Chem. Lett. 32 (2021) 1857–1868.
[7] F. Panza, M. Lozupone, G. Logroscino, B.P. Imbimbo, Nat. Rev. Neurol. 15 (2019) 73–88.
[8] K. Pietrzak, K. Czarnecka, E. Mikiciuk-Olasik, P. Szymanski, Med. Chem. 14 (2018) 34–43.
[9] N. Kumari, A. Kaul, R. Varshney, et al., Bioorgan. Chem. 111 (2021) 104972.
[10] N. Bandara, A.K. Sharma, S. Krieger, et al., J. Am. Chem. Soc. 139 (2017) 12550–12558.
[11] F. Mpambani, A.K.O. Aslund, F. Lerouge, et al., ACS Appl. Bio Mater. 1 (2018) 462–472.
[12] J. Miao, M. Miao, Y. Jiang, et al., Angew. Chem. Int. Ed. 62 (2023) e202216351.
[13] J. Yang, X. Wang, J. Liu, et al., Anal. Chem. 94 (2022) 15902–15907.
[14] X.Y. Liu, X.J. Wang, L. Shi, et al., Anal. Chem. 94 (2022) 7665–7673.
[15] H. Leng, Y. Wang, J. Wang, et al., Anal. Chem. 94 (2022) 1999–2006.
[16] J. Wu, C. Shao, X. Ye, et al., ACS Sens. 6 (2021) 863–870.
[17] L. Sun, H.J. Cho, S. Sen, et al., J. Am. Chem. Soc. 143 (2021) 10462–10476.
[18] J. Yang, B. Zhu, W. Yin, et al., Chem. Sci. 11 (2020) 5238–5245.
[19] J. Shin, P. Verwilst, H. Choi, et al., Angew. Chem. Int. Ed. 58 (2019) 5648–5652.
[20] J.Y. Zhu, L.F. Zhou, Y.K. Li, et al., Anal. Chim. Acta 961 (2017) 112–118.
[21] H. Fu, P. Tu, L. Zhao, et al., Anal. Chem. 88 (2016) 1944–1950.
[22] H. Fu, M. Cui, L. Zhao, et al., J. Med. Chem. 58 (2015) 6972–6983.
[23] M. Cui, M. Ono, H. Watanabe, et al., J. Am. Chem. Soc. 136 (2014) 3388–3394.
[24] H. Watanabe, M. Ono, K. Matsumura, et al., Mol. Imaging 12 (2013), doi:10.2310/7290.2013.00049.
[25] M. Ono, H. Watanabe, H. Kimura, H. Saji, ACS Chem. Neurosci. 3 (2012) 319–324.
[26] H. Benzeid, E. Mothes, E.M. Essassi, et al., CR Chim. 15 (2012) 79–85.
[27] D. Liu, D. Fu, L. Zhang, L. Sun, Chin. Chem. Lett. 32 (2021) 1066–1070.
[28] L. Sun, Y. Lei, Y. Wang, D. Liu, Chin. Chem. Lett. 33 (2022) 1946–1950.
[29] T. Zhang, X. Chen, C. Yuan, et al., Angew. Chem. Int. Ed. 62 (2023) e202211550.
[30] H. Li, J. Wang, Y. Li, et al., Sens. Actuators B: Chem. 358 (2022) 131481.
[31] J. An, P. Verwilst, H. Aziz, et al., Bioact. Mater. 13 (2022) 239–248.
[32] X. Mu, F. Wu, R. Wang, et al., Sens. Actuators B: Chem. 338 (2021).
[33] K. Zhou, C. Yuan, B. Dai, et al., J. Med. Chem. 62 (2019) 6694–6704.
[34] M. Xu, R. Li, X. Li, et al., J. Mater. Chem. B 7 (2019) 5535–5540.
[35] H. Tan, K. Zhou, J. Yan, et al., Sens. Actuators B: Chem. 298 (2019) 126903.
[36] W. Fu, C. Yan, Z. Guo, et al., J. Am. Chem. Soc. 141 (2019) 3171–3177.
[37] K. Zhou, Y. Li, Y. Peng, et al., Anal. Chem. 90 (2018) 8576–8582.
[38] W. Ren, J. Zhang, C. Peng, et al., Bioconjugate Chem. 29 (2018) 3459–3466.
[39] C. Chen, Z. Liang, B. Zhou, et al., ACS Chem. Neurosci. 9 (2018) 3128–3136.
[40] K. Zhou, H. Bai, L. Feng, et al., Anal. Chem. 89 (2017) 9432–9437.
[41] K. Rajasekhar, N. Narayanaswamy, N.A. Murugan, et al., Biosens. Bioelectron. 98 (2017) 54–61.
[42] Y. Li, J. Yang, H. Liu, et al., Chem. Sci. 8 (2017) 7710–7717.
[43] C.L. Teoh, D. Su, S. Sahu, et al., J. Am. Chem. Soc. 137 (2015) 13503–13509.
[44] S.V. Fedoseev, M.Y. Belikov, M.Y. Ievlev, Dyes Pigm. 204 (2022) 110455.
[45] S.V. Fedoseev, M.Y. Belikov, M.Y. Ievlev, et al., Dyes Pigm. 165 (2019) 451–457.
[46] K.A. Bertman, C.S. Abeywickrama, Y. Pang, ChemBioChem 23 (2022) e202100516.
[47] L. Guo, R. Zhang, Y. Sun, et al., Analyst 141 (2016) 3228–3232.
[48] T. Sachdeva, M.D. Milton, J. Photochem. Photobiol. A: Chem. 402 (2020) 112804.
[49] L. Gremer, D. Scholzel, C. Schenk, et al., Science 358 (2017) 116–119.
[50] Y. Zhao, S. Tian, J. Zhang, et al., Nano Today 44 (2022) 101457.